Journal of Mathematics in Industry
a SpringerOpen Journal

RESEARCH Open Access

Simulation of floating potentials in industrial applications by boundary element methods

Dominic Amann[1], Andreas Blaszczyk[2], Günther Of[1*] and Olaf Steinbach[1]

[*]Correspondence: of@tugraz.at
[1]Institut für Numerische Mathematik, Technische Universität Graz, Steyrergasse 30, Graz, 8010, Austria
Full list of author information is available at the end of the article

Abstract

We consider the electrostatic field computations with floating potentials in a multi-dielectric setting. A floating potential is an unknown equipotential value associated with an isolated perfect electric conductor, where the flux through the surface is zero. The floating potentials can be integrated into the formulations directly or can be approximated by a dielectric medium with high permittivity. We apply boundary integral equations for the solution of the electrostatic field problem. In particular, an indirect single layer potential ansatz and a direct formulation based on the Steklov-Poincaré interface equation are considered. All these approaches are discussed in detail and compared for several examples including some industrial applications. In particular, we will demonstrate that the formulations involving constraints are vastly superior to the penalized formulations with high permittivity, which are widely used in practice.

MSC: 65N38; 78A30

Keywords: electrostatic field computations; boundary element methods; industrial applications

1 Introduction

For the solution of 3D electrostatic field problems, boundary element methods are widely used and are, in particular, advantageous in the presence of an unbounded domain. In addition to Dirichlet and Neumann boundary conditions, so-called floating potentials may occur. Isolated perfect electric conductors result in equipotential surfaces. The equipotential value of the surface is unknown, but, in addition, the flux through the closed surface must be zero in the absence of sources. Such floating electrodes are found in, e.g., some lightning protection systems and can modify the breakdown probability of air gaps [1].

While there are numerous papers on the solution of electrostatic field problems with floating potentials by boundary element methods and related methods, like the charge simulation method [2, 3], in the engineering literature, a detailed view based on a mathematically profound basis seems to be missing. In this paper, we try to close this gap and, in addition, compare several formulations in practical examples. In particular, we consider boundary element methods, see, e.g., [4–6], for the solution of electrostatic field problems with floating potentials in a multi-dielectric setting. We apply an indirect approach based on the single layer potential and a domain decomposition method based on symmetric approximations of the local Dirichlet to Neumann maps, the so-called Steklov-Poincaré operators, see e.g. [7–10]. These two methods have been compared for magne-

tostatic problems in [11, 12]. Here, we apply these formulations for electrodes at floating potentials.

As electrodes at floating potentials can be considered equivalent to dielectric bodies with infinite permittivity, a common strategy is to substitute electrodes at floating potential by a dielectric media with high permittivity, see e.g. [13]. This approximation can be interpreted as a penalty approach. We compare this strategy to the direct incorporation of the constant but unknown potential and of the zero flux constraint into the formulations. While the penalty approach of a dielectric media with high permittivity needs no additional implementation work in a code which can cope with jumping permittivities, the approach with constraints is highly preferable from a mathematical point of view. Our numerical examples will demonstrate that the results of the approach with constraints are superior to the ones of the penalty approach. In addition, we will show that the formulations based on the Steklov-Poincaré interface equation have advantages over the single layer potential ansatz in case of corners and edges.

The paper is organized as follows: A model problem of the electrostatic field computation with floating potential is introduced in Section 2. In Section 3, the formulations based on the Steklov-Poincaré interface equation and the single layer potential ansatz are presented, and the unique solvability of the variational formulations is proven. The boundary element discretization of both formulations is described in Section 4, and first academic examples in Section 5 show the advantages and disadvantages of the considered approaches. Finally we discuss several extensions of the model problem and apply the methods to examples of industrial applications like an arrester, a bushing, and an insulator with partial wetting in Section 6.

2 Floating potentials in electrostatic field problems

We apply the scalar potential ansatz for the computation of an electrostatic field $\mathbf{E} = -\nabla\varphi$. We consider the union $\Omega_0 = \Omega_E \cup \Omega_F \cup \Omega_D$ of several disjoint Lipschitz domains, a domain Ω_E of an electrode, a domain Ω_F with a floating potential, and a dielectric domain Ω_D. In addition we define the exterior domain $\Omega_0^e = \mathbb{R}^3 \setminus \overline{\Omega}_0$. For the ease of presentation we assume that the intersection of the closures of any two domains Ω_E, Ω_F, and Ω_D is empty. We will comment on more general situations in Section 6. The model problem reads: Find a scalar potential φ such that $\varphi_D = \varphi_{|\Omega_D}$, $\varphi_0 = \varphi_{|\Omega_0^e}$, and a constant $\alpha = \varphi_{|\Omega_F}$ are the solution of

$$-\Delta\varphi_D(x) = 0 \quad \text{for } x \in \Omega_D, \tag{1}$$

$$-\Delta\varphi_0(x) = 0 \quad \text{for } x \in \Omega_0^e, \tag{2}$$

$$\varphi_0(x) = g \quad \text{for } x \in \Gamma_E := \partial\Omega_E, \tag{3}$$

$$\varphi_D(x) = \varphi_0(x) \quad \text{for } x \in \Gamma_D, \tag{4}$$

$$\varepsilon_D \frac{\partial}{\partial n_D}\varphi_D(x) = \varepsilon_0 \frac{\partial}{\partial n_D}\varphi_0(x) \quad \text{for } x \in \Gamma_D, \tag{5}$$

$$\varphi_0(x) = \mathcal{O}\big(|x|^{-1}\big) \quad \text{as } |x| \to \infty, \tag{6}$$

$$\varphi_0(x) = \alpha \quad \text{for } x \in \Gamma_F := \partial\Omega_F, \tag{7}$$

$$\int_{\Gamma_F} \frac{\partial}{\partial n_F}\varphi_0(x)\, ds_x = 0. \tag{8}$$

Here n_i denotes the exterior unit normal vector on $\Gamma_i := \partial\Omega_i$, $i \in \{0, D, E, F\}$, and is defined almost everywhere. On the surface Γ_E of the electrode a constant potential g is given in (3), while we enforce continuity of the potential as well as of the flux for the dielectrics by (4) and (5). In addition, we introduce Γ as the union of all boundaries. For our simple model problem $\Gamma = \Gamma_0$. Note that we distinguish Γ_0 and Γ from the beginning, such that the developed boundary integral equations can be applied to more general settings which are discussed in Section 6. The dielectric domain is characterized by its relative permittivity ε_D and the exterior domain Ω_0^c by ε_0. For the floating potential, we assume a constant but unknown potential α on the boundary Γ_F in (7), but the total flux through this surface is zero, see (8).

We will consider two approaches to solve such boundary value problems with a floating potential numerically. The first approach is to solve the boundary value problem in the form (1)-(8), taking into account the constant but unknown potential α and the constraint (8) directly. The second approach, which is widely used in practice due to its simple implementation, is to approximate the floating potential by considering Ω_F to be a dielectric medium with high relative permittivity ε_F, i.e., to determine a potential φ_F instead of α. In this case we end up with a system consisting of (1)-(6) with additional transmission conditions on Γ_F:

$$\varphi_F(x) = \varphi_0(x) \quad \text{for } x \in \Gamma_F, \tag{9}$$

$$\varepsilon_F \frac{\partial}{\partial n_F}\varphi_F(x) = \varepsilon_0 \frac{\partial}{\partial n_F}\varphi_0(x) \quad \text{for } x \in \Gamma_F. \tag{10}$$

We will demonstrate by some numerical examples in Section 5 that the penalty approach of an additional dielectric medium with a high relative permittivity gives bad approximations of the floating potential in general.

3 Boundary integral equations

If we use $\Gamma_C = \Gamma \setminus \Gamma_E = \Gamma_D \cup \Gamma_F$ instead of Γ_D in (4) and (5) and set the permittivities ε correctly, the model with a high relative permittivity ε_F is the special case (1)-(6) of the full model (1)-(8) with a floating potential. Thus we will derive the boundary integral equations for the full model only. For the model with a high relative permittivity we just need to drop the boundary integral equations related to Γ_F and take into account the ones of Γ_D for Γ_F in addition.

We consider an approach which is based on the Steklov-Poincaré interface equation known from domain decomposition methods, see e.g. [14, 15], and an indirect ansatz leading to a single layer boundary integral equation. While the latter approach is popular due to the ease of implementation, the domain decomposition approach will result in better approximations for the examples in Sections 5 and 6.

3.1 Steklov-Poincaré interface equation

The solutions of the Laplace equations (1) and (2) are given by the representation formulae

$$\varphi_D(x) = \int_{\Gamma_D} U^*(x,y) t_D(y)\, ds_y - \int_{\Gamma_D} \frac{\partial}{\partial n_{D,y}} U^*(x,y)\varphi_D(y)\, ds_y \quad \text{for } x \in \Omega_D,$$

$$\varphi_0(x) = -\int_{\Gamma_0} U^*(x,y) t_0(y)\, ds_y + \int_{\Gamma_0} \frac{\partial}{\partial n_{0,y}} U^*(x,y)\varphi_0(y)\, ds_y \quad \text{for } x \in \Omega_0^c,$$

with $t_D := \frac{\partial}{\partial n_D}\varphi_D$, $t_0 := \frac{\partial}{\partial n_0}\varphi_0$, and the fundamental solution

$$U^*(x,y) = \frac{1}{4\pi}\frac{1}{|x-y|}.$$

Thus we need to determine the unknown parts of the Cauchy data $[t_i, \varphi_i]$, $i \in \{0, D\}$.

The interior Steklov-Poincaré operator $S^D : H^{1/2}(\Gamma_D) \to H^{-1/2}(\Gamma_D)$ maps some given Dirichlet datum φ_D onto the related Neumann datum $t_D = S^D\varphi_D$ of the corresponding solution of the Laplace equation (1). Analogously the exterior Steklov-Poincaré operator $S^0 : H^{1/2}(\Gamma_0) \to H^{-1/2}(\Gamma_0)$ gives $t_0 = -S^0\varphi_0$. These two operators can be defined in their so-called symmetric representation, see e.g. [6, Section 6.6.3, p. 148], by

$$S^D = D_D + \left(\frac{1}{2}I + K_D'\right)V_D^{-1}\left(\frac{1}{2}I + K_D\right),$$
$$S^0 = D_0 + \left(\frac{1}{2}I - K_0'\right)V_0^{-1}\left(\frac{1}{2}I - K_0\right).$$

The single layer boundary integral operator V_i, the double layer boundary integral operator K_i, its adjoint K_i', and the hypersingular operator D_i are defined with respect to Γ_i, $i \in \{0, D, E, F\}$, by

$$(V_i t_i)(x) = \int_{\Gamma_i} U^*(x,y)t_i(y)\,ds_y,$$
$$(K_i\varphi_i)(x) = \int_{\Gamma_i} \frac{\partial}{\partial n_{i,y}}U^*(x,y)\varphi_i(y)\,ds_y,$$
$$\left(K_i' t_i\right)(x) = \int_{\Gamma_i} \frac{\partial}{\partial n_{i,x}}U^*(x,y)\varphi_i(y)\,ds_y,$$
$$(D_i\varphi_i)(x) = -\frac{\partial}{\partial n_{i,x}}\int_{\Gamma_i} \frac{\partial}{\partial n_{i,y}}U^*(x,y)\varphi_i(y)\,ds_y.$$

As the two Steklov-Poincaré operators S^D and S^0 correspond to the solution of local Dirichlet boundary value problems, it remains to satisfy the boundary and transmission conditions. We need to find a global function $\varphi \in H^{1/2}(\Gamma)$ such that

$$\varphi(x) = g \quad \text{for } x \in \Gamma_E, \qquad \varphi(x) = \alpha \quad \text{for } x \in \Gamma_F,$$

i.e., the boundary conditions (3) and (7) as well as the transmission condition (4) are satisfied. Using $t_0 = -S^0\varphi$, $t_D = S^D\varphi_{|\Gamma_D}$, and the splitting $\varphi = \varphi_D + g1_E + \alpha 1_F$, where $1_i(x) = 1$ for $x \in \Gamma_i$ and 0 else, the remaining transmission condition (5) and the constraint (8) result in the final system: Find $\varphi_D \in H^{1/2}(\Gamma_D)$ and $\alpha \in \mathbb{R}$ such that

$$\left(\varepsilon_D S^D + \varepsilon_0 S^0\right)\varphi_D(x) + \alpha\varepsilon_0\left(S^0 1_F\right)(x) = -g\varepsilon_0\left(S^0 1_E\right)(x) \quad \text{for } x \in \Gamma_D, \tag{11}$$
$$\int_{\Gamma_F}\left(\left(S^0\varphi_D\right)(x) + \alpha\left(S^0 1_F\right)(x)\right)ds_x = -g\int_{\Gamma_F}\left(S^0 1_E\right)(x)\,ds_x. \tag{12}$$

3.2 Single layer boundary integral operator formulation

Due to its popularity in practice, see [16] and references given therein, we consider a global single layer potential ansatz by

$$\varphi(x) = \int_\Gamma U^*(x,y)w(y)\,ds_y \quad \text{for } x \in \mathbb{R}^3 \setminus \Gamma$$

for any single layer charge density $w \in H^{-1/2}(\Gamma)$ for the global solution φ of the boundary value problem (1)-(8). With this choice the local partial differential equations (1) and (2), the continuity condition (4) as well as the radiation condition (6) are satisfied. The remaining Dirichlet boundary condition (3), the floating potential condition (7), the flux transmission condition (5), and the scaling condition (8) provide the equations to determine the unknown density $w \in H^{-1/2}(\Gamma)$:

$$(Vw)(x) = g \quad \text{for } x \in \Gamma_E, \tag{13}$$

$$(Vw)(x) - \alpha = 0 \quad \text{for } x \in \Gamma_F, \tag{14}$$

$$\frac{1}{2}\frac{\varepsilon_D + \varepsilon_0}{\varepsilon_D - \varepsilon_0} w(x) + \big(K'w\big)(x) = 0 \quad \text{for almost all } x \in \Gamma_D, \tag{15}$$

$$\int_{\Gamma_F} \left(-\frac{1}{2} w(x) + \big(K'w\big)(x) \right) ds_x = 0, \tag{16}$$

where V denotes the global single layer boundary integral operator and K' is the global adjoint double layer boundary integral operator for $x \in \Gamma$:

$$(Vw)(x) = \int_\Gamma U^*(x,y)w(y)\,ds_y, \qquad \big(K'w\big)(x) = \int_\Gamma \frac{\partial}{\partial n_x} U^*(x,y)w(y)\,ds_y.$$

3.3 Unique solvability

Lemma 3.1 *There exists a unique solution* $(\varphi_D, \alpha) \in H^{1/2}(\Gamma_D) \times \mathbb{R}$ *satisfying* (11)-(12).

Proof Using the splitting $\varphi = \varphi_D + \alpha 1_F + g1_E$, we can reformulate (11)-(12) as: Find $\varphi \in X := \{\psi \in H^{1/2}(\Gamma) : \psi_{|\Gamma_F} = \alpha, \alpha \in \mathbb{R}, \psi_{|\Gamma_E} = 0\}$:

$$\big\langle \big(\varepsilon_D S^D + \varepsilon_0 S^0\big)\varphi, \psi \big\rangle_\Gamma = -\big\langle g\varepsilon_0 S^0 1_E, \psi \big\rangle_\Gamma \quad \text{for all } \psi \in X.$$

This variational formulation admits a unique solution, as $X \subset H^{1/2}(\Gamma)$, the exterior Steklov-Poincaré operator S^0 is $H^{1/2}(\Gamma)$-elliptic, and the interior Steklov-Poincaré operator S^D is $H^{1/2}(\Gamma_D)$-semi-elliptic, see, e.g., [14, Lemma 1.83, p. 49f] and [6, Section 6.6.3, p.149]. □

Lemma 3.2 *Let* $(\varphi_D, \alpha) \in H^{1/2}(\Gamma_D) \times \mathbb{R}$ *be a solution of the Steklov-Poincaré interface equations* (11)-(12), *and let* $w \in H^{-1/2}(\Gamma)$ *be a solution of the indirect single layer approach* (13)-(16). *Then there holds the relation*

$$\varphi(x) = \varphi_D(x) + \alpha 1_F(x) + g1_E(x) = (Vw)(x) \quad \textit{for } x \in \Gamma.$$

Proof Obviously, the statement holds true for all $x \in \Gamma_E$, as the condition (13) for the single layer potential approach coincide with the choice of φ for the Steklov-Poincaré interface

equation. On Γ_F the assertion holds true due to (14). On Γ_D we start from the continuity (15) of the flux for the single layer potential approach, use $w = V^{-1}Vw$ and the symmetry relation $K'V^{-1} = V^{-1}K$, see e.g. [6, Corollary 6.19, p.138],

$$\begin{aligned} 0 &= \varepsilon_D\left(\frac{1}{2}I + K'\right)w(x) + \varepsilon_0\left(\frac{1}{2}I - K'\right)w(x) \\ &= \varepsilon_D V^{-1}\left(\frac{1}{2}I + K\right)Vw(x) + \varepsilon_0 V^{-1}\left(\frac{1}{2}I - K\right)Vw(x) \quad \text{for } x \in \Gamma_D. \end{aligned}$$

For the first term $u = V^{-1}(\frac{1}{2}I + K)z$ we can apply some simplifications using the splitting of the functions and operators

$$\begin{aligned} &(V_D u_D)(x) + (V_E u_E)(x) + (V_F u_F)(x) \\ &\quad = \frac{1}{2}z_D(x) + (K_D z_D)(x) + (K_E z_E)(x) + (K_F z_F)(x) \end{aligned}$$

for almost all $x \in \Gamma_D$, which reduces to

$$(V_D u_D)(x) = \left(\frac{1}{2}I + K_D\right)z_D(x) \quad \text{for almost all } x \in \Gamma_D$$

because there holds

$$(V_i t_i)(x) - (K_i z_i)(x) = 0 \quad \text{for } x \in \Omega_i^c, i \in \{E, F\},$$

for any solution z_i and $t_i = \frac{\partial z_i}{\partial n_i}$ of the local Laplace equations. With the so-called non-symmetric representations $S^D = V_D^{-1}(\frac{1}{2}I + K_D)$ and $S^0 = V_0^{-1}(\frac{1}{2}I - K_0)$ of the Steklov-Poincaré operators we end up with

$$\varepsilon_D S^D(Vw)(x) + \varepsilon_0 S^0(Vw)(x) = 0 \quad \text{for } x \in \Gamma_D.$$

Applying the same technique for the constraint (16) of the single layer potential ansatz, we end up with

$$\int_{\Gamma_F} S^0(Vw)(x)\, ds_x = 0.$$

Taking into account the floating potential (14), these two equations coincide with the formulation (11)-(12) of the Steklov-Poincaré interface equation, and hence we conclude $\varphi = Vw$ on Γ. □

Due to equivalence of the two formulations we conclude the unique solvability of the indirect approach (13)-(16) from Lemma 3.1.

4 Boundary element methods

For the discretization of the considered boundary integral formulations, we assume a quasi-uniform mesh of the surface Γ with N plane triangles and M nodes. The considered trial and ansatz spaces are the space $S_h^0(\Gamma) = \operatorname{span}\{\psi_\ell^0\}_{\ell=1}^N$ of piecewise constant functions and the space $S_h^1(\Gamma) = \operatorname{span}\{\psi_\ell^1\}_{\ell=1}^M$ of piecewise linear and continuous functions. We

use Galerkin variational formulations for the discretization of the domain decomposition method (11)-(12) and of the single layer boundary integral equations (13)-(16).

4.1 Steklov-Poincaré interface equation

We transfer the splitting $\varphi = \varphi_D + \alpha 1_F + g 1_E$ of the solution of (11)-(12) to the Steklov-Poincaré operators such that S^0_{ij} indicates that the operator S^0 is applied to a function defined on Γ_j only and evaluated on Γ_i for $i,j \in \{D,E,F\}$.

Thus the discrete Galerkin variational formulation of (11)-(12) is to find $(\varphi_{D,h},\alpha) \in S^1_h(\Gamma_D) \times \mathbb{R}$ such that

$$\begin{aligned}
&\left\langle \left(\varepsilon_D S^D_{DD} + \varepsilon_0 S^0_{DD}\right)\varphi_{D,h}, \nu_h \right\rangle_{\Gamma_D} + \alpha\varepsilon_0 \left\langle S^0_{DF} 1_F, \nu_h \right\rangle_{\Gamma_D} = -\varepsilon_0 g \left\langle S^0_{DE} 1_E, \nu_h \right\rangle_{\Gamma_D}, \\
&\varepsilon_0 \left\langle S^0_{FD}\varphi_{D,h}, 1_F \right\rangle_{\Gamma} + \alpha\varepsilon_0 \left\langle S^0_{FF} 1_F, 1_F \right\rangle_{\Gamma} = -\varepsilon_0 g \left\langle S^0_{FE} 1_E, 1_F \right\rangle_{\Gamma}
\end{aligned}$$

for all $\nu_h \in S^1_h(\Gamma_D)$. Due to the inverse of the single layer potential, a direct computation of S^0 and S^D is not possible in general. But we can use the approximations

$$\begin{aligned}
S^D_h &:= D_{D,h} + \left(\frac{1}{2}M^\top_{D,h} + K^\top_{D,h}\right) V^{-1}_{D,h} \left(\frac{1}{2}M_{D,h} + K_{D,h}\right), \\
S^0_h &:= D_{0,h} + \left(\frac{1}{2}M^\top_{0,h} - K^\top_{0,h}\right) V^{-1}_{0,h} \left(\frac{1}{2}M_{0,h} - K_{0,h}\right).
\end{aligned}$$

These approximations are symmetric, positive semi-definite, and positive definite, respectively. The additional error caused by these approximations features the same quasi-optimal order of convergence as the Galerkin approximations of the exact operators, see e.g. [6, Lemma 12.11]. Thus, there is no substantial loss of accuracy. The Galerkin matrices are given by

$$\begin{aligned}
D_{i,h}[k,\ell] &= \left\langle D_i \psi^1_\ell, \psi^1_k \right\rangle_{\Gamma_i}, \qquad V_{i,h}[m,n] = \left\langle V_i \psi^0_n, \psi^0_m \right\rangle_{\Gamma_i}, \\
K_{i,h}[m,\ell] &= \left\langle K_i \psi^1_\ell, \psi^0_m \right\rangle_{\Gamma_i}, \qquad M_{i,h}[m,\ell] = \left\langle \psi^1_\ell, \psi^0_m \right\rangle_{\Gamma_i}
\end{aligned}$$

for $k,\ell = 1,\dots,M_i$; $m,n = 1,\dots,N_i$, and $i \in \{D,E,F\}$. Finally, we have to solve the following system of linear equations

$$\begin{pmatrix} \varepsilon_D S^D_{DD,h} + \varepsilon_0 S^0_{DD,h} & \underline{a} \\ \underline{a}^\top & \lambda \end{pmatrix} \begin{pmatrix} \underline{\varphi}_D \\ \alpha \end{pmatrix} = \begin{pmatrix} \underline{f}_D \\ f_F \end{pmatrix}, \tag{17}$$

where

$$\underline{a}[\ell] := \varepsilon_0 \left\langle S^0_{DF,h} 1_F, \psi^1_\ell \right\rangle_{\Gamma_D}, \qquad \lambda := \varepsilon_0 \left\langle S^0_{FF,h} 1_F, 1_F \right\rangle_{\Gamma_F}.$$

Due to the positive semi-definiteness of S^D_h and the positive definiteness of S^0_h the linear system (17) is uniquely solvable, see Lemma 3.1.

For the approach which approximates the floating potential by considering Ω_F to be a dielectric with a high relative permittivity ε_F, we have to solve the following system of

linear equations

$$\begin{pmatrix} \varepsilon_D S^D_{DD,h} + \varepsilon_0 S^0_{DD,h} & \varepsilon_0 S^0_{DF,h} \\ \varepsilon_0 S^0_{FD,h} & \varepsilon_F S^F_{FF,h} + \varepsilon_0 S^0_{FF,h} \end{pmatrix} \begin{pmatrix} \underline{\varphi}_D \\ \underline{\varphi}_F \end{pmatrix} = \begin{pmatrix} \underline{f}_D \\ \underline{f}_F \end{pmatrix}. \tag{18}$$

The unique solvability of both discrete formulations (17) and (18) is a consequence of the positive definiteness of the approximation S^0_h of the exterior Steklov-Poincaré operator S^0 and the positive semi-definiteness of the approximation S^i_h of the other Steklov-Poincaré operator S^i ($i \in \{D, F\}$), see, e.g., [14, Lemma 1.93, p.58f] and [6, Lemma 12.11, p.285].

4.2 Single layer boundary integral operator formulation

We use piecewise constant functions from $S^0_h(\Gamma)$ as test and ansatz functions in the system (13)-(16). As before we apply the splitting of the unknown density $w_h \in S^0_h(\Gamma)$ into $(w_{F,h}, w_{E,h}, w_{D,h}) \in S^0_h(\Gamma_F) \times S^0_h(\Gamma_E) \times S^0_h(\Gamma_D)$. So the discrete variational formulation of the single layer boundary integral operator formulation (13)-(16) is to find $(w_{F,h}, w_{E,h}, w_{D,h}, \alpha) \in S^0_h(\Gamma_F) \times S^0_h(\Gamma_E) \times S^0_h(\Gamma_D) \times \mathbb{R}$ such that

$$\begin{aligned} \langle V_{EF} w_{F,h} + V_{EE} w_{E,h} + V_{ED} w_{D,h}, \psi_E \rangle_{\Gamma_E} &= g \langle 1_E, \psi_E \rangle_{\Gamma_E}, \\ \langle V_{FF} w_{F,h} + V_{FE} w_{E,h} + V_{FD} w_{D,h}, \psi_F \rangle_{\Gamma_F} - \alpha \langle 1_F, \psi_F \rangle_{\Gamma_F} &= 0, \\ \left\langle K'_{DF} w_{F,h} + K'_{DE} w_{E,h} + K'_{DD} w_{D,h}, \psi_D \right\rangle_{\Gamma_D} + \tfrac{1}{2} \tfrac{\varepsilon_D + \varepsilon_0}{\varepsilon_D - \varepsilon_0} \langle w_{D,h}, \psi_D \rangle_{\Gamma_D} &= 0, \\ \left\langle K'_{FF} w_{F,h} + K'_{FE} w_{E,h} + K'_{FD} w_{D,h}, 1_F \right\rangle_{\Gamma_F} - \tfrac{1}{2} \langle w_{F,h}, 1_F \rangle_{\Gamma_F} &= 0, \end{aligned} \tag{19}$$

for all test functions $\psi_i \in S^0_h(\Gamma_i)$ for $i \in \{F, E, D\}$. In the considered geometric setting, the equation (19) allows for some simplification utilizing the adjointness and the kernel properties of the double layer potential operator:

$$\begin{aligned} 0 &= \left\langle K'_{FF} w_{F,h} + K'_{FE} w_{E,h} + K'_{FD} w_{D,h}, 1_F \right\rangle_{\Gamma_F} - \frac{1}{2} \langle w_{F,h}, 1_F \rangle_{\Gamma_F} \\ &= \langle w_{F,h}, K_{FF} 1_F \rangle_{\Gamma_F} - \frac{1}{2} \langle w_{F,h}, 1_F \rangle_{\Gamma_F} = -\langle w_{F,h}, 1_F \rangle_{\Gamma_F}. \end{aligned}$$

This formulation is equivalent to the following system of linear equations

$$\begin{pmatrix} V_{EE,h} & V_{EF,h} & V_{ED,h} & \\ V_{FE,h} & V_{FF,h} & V_{FD,h} & -\underline{b} \\ \widetilde{K}^\top_{DE,h} & \widetilde{K}^\top_{DF,h} & \frac{1}{2} \frac{\varepsilon_D + \varepsilon_0}{\varepsilon_D - \varepsilon_0} \widetilde{M}_h + \widetilde{K}^\top_{DD,h} & \\ & \underline{b}^\top & & \end{pmatrix} \begin{pmatrix} \underline{w}_E \\ \underline{w}_F \\ \underline{w}_D \\ \alpha \end{pmatrix} = \begin{pmatrix} \underline{f}_E \\ \underline{0} \\ \underline{0} \\ 0 \end{pmatrix}, \tag{20}$$

where

$$\begin{aligned} V_{ij,h}[m,n] &= \left\langle V_j \psi^0_n, \psi^0_m \right\rangle_{\Gamma_i}, \qquad \widetilde{K}_{ij,h}[m,n] = \left\langle K_j \psi^0_n, \psi^0_m \right\rangle_{\Gamma_i}, \\ \widetilde{M}_{ij,h}[m,n] &= \left\langle \psi^0_n, \psi^0_m \right\rangle_{\Gamma_i}, \qquad \underline{b}[m] = \left\langle \psi^0_m, 1_F \right\rangle_{\Gamma_F} \end{aligned}$$

for $i, j \in \{D, E, F\}$, $m, n = 1, \ldots, N_i$ or N_j.

For the approach which approximates the floating potential by considering Ω_F as a dielectric with a high relative permittivity ε_F, the corresponding system reads

$$\begin{pmatrix} V_{EE,h} & V_{EF,h} & V_{ED,h} \\ \widetilde{K}_{FE,h}^{\top} & \frac{1}{2}\frac{\varepsilon_F+\varepsilon_0}{\varepsilon_F-\varepsilon_0}\widetilde{M}_h + \widetilde{K}_{FF,h}^{\top} & \widetilde{K}_{FD,h}^{\top} \\ \widetilde{K}_{DE,h}^{\top} & \widetilde{K}_{DF,h}^{\top} & \frac{1}{2}\frac{\varepsilon_D+\varepsilon_0}{\varepsilon_D-\varepsilon_0}\widetilde{M}_h + \widetilde{K}_{DD,h}^{\top} \end{pmatrix} \begin{pmatrix} \underline{w}_E \\ \underline{w}_F \\ \underline{w}_D \end{pmatrix} = \begin{pmatrix} \underline{f}_E \\ \underline{0} \\ \underline{0} \end{pmatrix}. \tag{21}$$

To our best knowledge, the stability of these indirect boundary element formulations is still an open problem for general Lipschitz surfaces due to the inconsistent, but widely used discretization of the adjoint double layer potential in $L_2(\Gamma)$.

5 Numerical examples

In this section, we consider a few rather academic examples to compare the introduced approaches to solve the electrostatic potential problem (1)-(8). We compare four formulations in total. We apply the Steklov-Poincaré (SP) operator formulation (18) and the indirect single layer potential (SL) ansatz (21) for the full dielectric approach (full dielectric) with a high relative permittivity $\varepsilon_F = 10{,}000$ to approximate the floating potential. For the direct incorporation (floating) of the floating potential we solve the Steklov-Poincaré (SP) system (17) and the indirect single layer potential (SL) ansatz (20), respectively.

For the computations, we used an implementation [17] of the proposed boundary element methods which is based on the Fast Multipole Method [18] for fast and data-sparse realizations of the involved boundary integral operators. The Steklov-Poincaré operator formulation is implemented by means of MPI and we used one process per active subdomain, i.e. two processes for (17) and three processes for (18). The implementation of the Fast Multipole Method utilizes OpenMP and we used two threads for each instance of the program. The computations were done on a Workstation with 2 Intel Xeon E5620 processors and 24 GB RAM.

We use the concept of operators of opposite order [19] for the preconditioning of the Steklov-Poincaré operator formulations (17) and (18). We apply the artificial multilevel preconditioning [20, 21] for the inner inversion of the Galerkin matrix of the single layer boundary integral operator in the Steklov-Poincaré operator formulations. For the systems (20) and (21) of the indirect single layer potential ansatz, we use the artificial multilevel preconditioning for the block of the single layer boundary integral operator and a diagonal scaling for the block of the adjoint double layer potential operator.

5.1 Two spheres

The two spheres of our first example [22] have the same diameter which is twice the distance of the two spheres. The first sphere Ω_E is an electrode with a given potential of $\varphi = g = 100$ on its surface. The second sphere Ω_F is either a floating potential or a dielectric with relative permittivity $\varepsilon_F = 10{,}000$, depending on the considered approach. The surrounding air has the relative permittivity $\varepsilon_0 = 1$.

In Table 1, we provide the approximations of the floating potential α and the computational times of the four formulations for several refinement levels. For this setting an approximate solution of an axial symmetric charge simulation solver (ELFI, [23]) is used for comparison. One purpose of the new solvers is to overcome the restrictions of ELFI to axial symmetric geometries. For the full dielectric approach, we do not determine α

Table 1 Approximate values of the floating potential α on Γ_F and computational times for the example of two spheres

Number of elements	256		1,040		4,160	
SP floating	32.41	1 s	33.63	8 s	33.86	35 s
SL floating	32.41	1 s	33.63	4 s	33.86	20 s
SP full dielectric	32.40	2 s	33.62	12 s	33.85	50 s
SL full dielectric	32.39	1 s	33.62	5 s	33.86	28 s
2D ELFI			33.9			

Table 2 Approximate values of the floating potential α on Γ_F and computational times for the example of a sphere and a bicone

Number of elements	384		1,536		6,144		24,576	
SP floating	44.512	2 s	45.339	15 s	45.572	79 s	45.637	329 s
SL floating	44.512	2 s	45.341	7 s	45.573	28 s	45.637	124 s
SP full dielectric	44.512	3 s	45.340	27 s	45.573	106 s	45.636	569 s
SL full dielectric	44.433	2 s	45.355	11 s	45.553	34 s	45.632	168 s
2D ELFI				45.7				

Table 3 Range of the floating potential φ_F for the sphere and the bicone

Number of elements	384	1,536	6,144	24,576
SP full dielectric	44.51-44.53	45.33-45.36	45.55-45.59	45.62-45.65
SL full dielectric	40.38-61.91	42.34-58.26	43.34-54.93	44.02-52.41

directly but provide the mean value of the potential on Γ_F. Even on the finest refinement level the potential φ_F is not constant, it has a range of 0.1983 for the indirect approach and 0.0209 for the Steklov-Poincaré operator formulation.

We notice that all four formulations result in good and similar approximate solutions. Only the indirect single layer formulation (21) for the full dielectric model gives a potential which is not quite constant although we consider approximations of smooth objects. We will encounter this behavior to a greater extend in the next example.

5.2 Sphere and bicone

Now we consider an example consisting of a sphere and a bicone [22]. Both have the same diameter and are arranged at a distance of one eighth of their diameter. One spike of the bicone points towards the sphere. The sphere Ω_E is an electrode with a given potential $\varphi = g = 100$. The bicone Ω_F has a floating potential and the exterior domain has a relative permittivity of $\varepsilon_0 = 1$. In Table 2, we present the approximations of the floating potential α and the computational times. Again an approximate solution of the potential on the surface Γ_F of the cone by an axial symmetric FEM solver is used for comparison.

Note that the mean value of the potential on the surface Γ_F is given for the full dielectric approaches. Therefore we analyze the range of φ_F for these approaches in Table 3 in details. The Steklov-Poincaré operator formulation gives an almost constant potential φ_F on the whole surface Γ_F. But we observe that the potential varies strongly for the single layer potential ansatz, even more than in the last example. The extremal values are taken at the spikes of the bicone. Such a behavior like artificial singularities can be observed for geometries with corners and edges and results in significant loss of accuracy, see, e.g., [11, 12]. The computational times of the formulations related to the Steklov-Poincaré interface

equation are higher than those of the single layer potential ansatz for the same mesh, but we neglect the accuracy of the approximations (see results for 'SL full dielectric' in Table 3) in this comparison.

6 Extensions and applications

We observed poor approximations by the single layer potential ansatz for large jumps in the permittivities ε in the example of the sphere and the bicone due to artificial singularities in the discrete solution, see the formulation 'SL full dielectric' in Table 3. For such simple examples the single layer potential ansatz with direct realization of the floating potential ('SL floating') gives still good results. But for examples with large jumps of the coefficients ε_D and ε_0 this is not the case anymore. As the third row in (20) is similar to the second and third row in (21), we are facing the same problem as for the formulation 'SL full dielectric' in Table 3. We observed these problems with artificial singularities in the discrete solution in the presence of dielectric media already for relative permittivity ε_D of 800 and higher, see e.g. [11, 12].

But for more general examples we have to cope with such jumps in the relative permittivities. In such cases, the approximation error of the single layer approach is more than one order of magnitude larger than the one of the Steklov-Poincaré operator formulations for the same mesh, see [11, 12]. Thus one needs significantly finer meshes for the single layer potential ansatz to come up with the same accuracy for this class of problems. This results in larger computational times than for the Steklov-Poincaré operator formulations. Due to these significant drawbacks of the single layer potential ansatz, we will consider the Steklov-Poincaré operator formulations only.

For real world examples, we need to consider more general settings. For the ease of presentation we have restricted the description of the formulations to one representative of each kind of subdomains and to well separated subdomains. We will now comment on some extensions.

The extension to several electrodes and dielectric subdomains is straightforward. For each boundary Γ_{F_i} and Γ_{D_i} the corresponding boundary integral equations (11), (12), and (14)-(16), respectively, have to be considered separately. For each floating subdomain Γ_{F_i} a separate degree of freedom α_i and the corresponding constraint

$$\int_{\Gamma_{F_i}} \frac{\partial}{\partial n_{F_i}} \varphi(x)\, ds_x = 0$$

have to be incorporated.

If two subdomains are in contact, we have to make some additional modifications. If a dielectric subdomain is in contact with an electrode, we use a discrete extension $\widetilde{g}$ of the given potential g to the surface Γ_D of the dielectric and determine the unknown remainder $\varphi_D - \widetilde{g}$ of φ_D. If the floating potential is surrounded by a dielectric medium instead of the exterior air domain the vector $\underline{a}$ and the coefficient λ in (17) involve $\varepsilon_D S^D$ instead of $\varepsilon_0 S^0$. In (18), $\varepsilon_D S^D$ and $\varepsilon_0 S^0$ are interchanged.

If Ω_F has interfaces to more than one subdomain, the constraint of the floating potential has to be taken with care. In the case of an interface to Ω_D and to the exterior domain Ω_0^c, the constraint reads as

$$\varepsilon_D \int_{\Gamma_F \cap \Gamma_D} \frac{\partial}{\partial n_F} \varphi_D(x)\, ds_x + \varepsilon_0 \int_{\Gamma_F \cap \Gamma_0} \frac{\partial}{\partial n_F} \varphi_0(x)\, ds_x = 0.$$

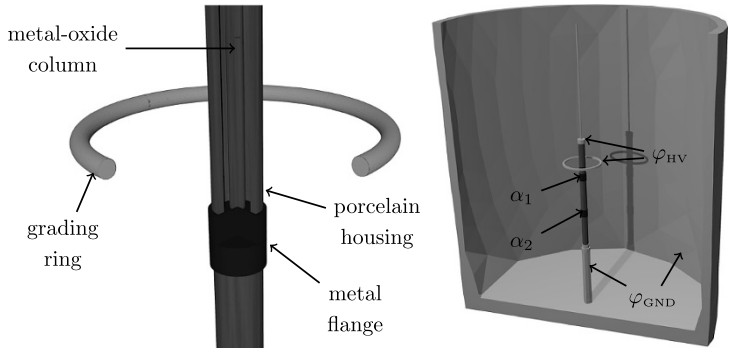

Figure 1 IEC arrester: the gray shades indicate the subdomains.

Table 4 Approximate values of the floating potentials and computational times for the IEC arrester

	α_1	α_2	Time
SP floating	57.44	24.28	4,559 s
SP full dielectric	57.41	24.23	9,659 s
2D ELFI	57.62	24.42	

This extended constraint can be transferred straightforward to the approach of the Steklov-Poincaré interface equation by the means of the related Steklov-Poincaré operators. For the indirect single layer potential ansatz, the simplification of the related constraint (19) seems not to be possible in general.

6.1 IEC arrester

The two remaining Steklov-Poincaré operator formulations are compared for the computation of the electric potential of the IEC surge arrester [24, Annex L] shown in Figure 1. Each of the three sections of the arrester (gray) consists of a metal-oxide cylindrical column with the equivalent relative permittivity $\varepsilon_D = 800$ surrounded by a porcelain housing with the relative permittivity $\varepsilon_D = 5$. In between the two dielectric domains there is a layer of air. The three sections are separated by two metal flanges (dark gray) at floating potentials. At the light gray parts the potential is given. The pedestal and the large surrounding cylinder are grounded electrodes with potential $\varphi_{\mathrm{GND}} = 0$. The top high voltage lead and the toroidal grading ring are electrodes with potential $\varphi_{\mathrm{HV}} = 100$. The exterior domain and the air inside the porcelain housing are modeled as dielectrics with $\varepsilon = 1$.

The difficulties in numerical 3D computations of the IEC arrester are related to the high permittivity of the metal-oxide as well as to the large differences between the radial and axial dimensions. Therefore, the accuracy of the potential computations using different approaches (FEM versus BEM or 2D versus 3D) is typically in the range of 2% as indicated in [24, Annex L]. The results in Table 4 show that the accuracy can be improved with the new Steklov-Poincaré operator formulation to the level of 0.5% (in spite of a relatively rough mesh). The values of the solution on the two floating potentials and the computational times are given in Table 4 for a surface mesh of 32,939 global nodes. As in the previous examples we observe a significant decrease of the computational time for the direct realization of the floating potential, while the solutions of the two approaches do not differ much. Therefore we dismiss the full dielectric model for the next examples.

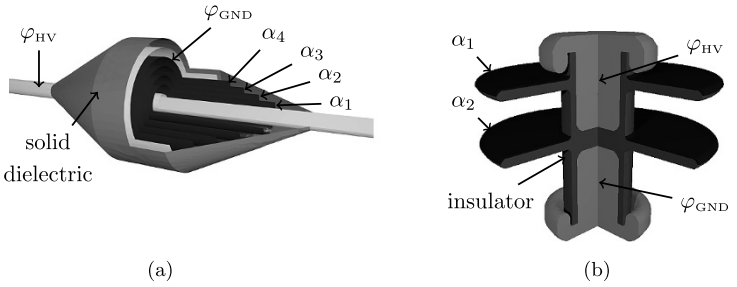

Figure 2 Geometric settings of (a) the bushing and (b) the partially wet insulator.

Table 5 Approximate values of the floating potentials for the bushing

	α_1	α_2	α_3	α_4
SP floating	70.7	51.4	35.1	19.0
2D ELFI	70.8	51.4	35.0	18.9

6.2 Bushing

The next example models a high voltage bushing [23] shown in Figure 2(a). It consists of a cylindrical conductor (light gray) with potential $\varphi_{\mathrm{HV}} = 100$ surrounded by five thin metallic foils embedded in a solid dielectric material (gray) with the relative permittivity $\varepsilon_D = 5$. The most outer foil (light gray) is grounded $\varphi_{\mathrm{GND}} = 0$ while the other four foils (dark gray) are at floating potentials. The role of the floating foils is enforcing a uniform potential distribution along the conical surface of the bushing. The difficult aspect of modeling bushings is the small thickness of the foils: for the bushing in Figure 2(a) the ratio between the foil thickness and its axial length is in the range of 10^{-3}. The computational mesh consists of 7,936 global nodes. Consequently the distance between elements created on the parallel foil surfaces is approximately 100 times smaller than the size of the elements. In spite of these extreme geometrical relations the floating potentials calculated for all foils with the Steklov-Poincaré operator approach show a good agreement with the 2D solution as presented in Table 5. The system (17) of linear equations is solved in 31 steps of a preconditioned CG method to a relative accuracy of 10^{-6}.

6.3 Insulator with partial wetting

The last example as depicted in Figure 2(b) is an insulator with embedded electrodes (light gray) at potentials $\varphi_{\mathrm{HV}} = 100$ and $\varphi_{\mathrm{GND}} = 0$. The relative permittivity of the insulator (gray) is $\varepsilon_D = 5$. The upper surface of both insulator sheds is covered by a water layer (dark gray). For the operational frequency of 50-60 Hz water behaves like a conducting material and can be approximated for a capacitive electrostatic field computation as an electrode. Consequently, the two very thin domains of water (dark gray) on the insulator sheds are modeled as electrodes at floating potentials. The geometrical dimensions of this arrangement are given in Table 6.

The solution of the floating version of the Steklov-Poincaré operator approach and the 2D solution are presented in Table 7. The computational mesh consists of 7,936 global nodes, and the system (17) of linear equations is solved in 49 steps of a preconditioned CG method to a relative accuracy of 10^{-6}.

Table 6 Geometrical dimensions of the insulator with partial wetting

Quantity	In mm
Electrodes distance	14
Insulation thickness between electrode and air	5
Shed diameter	160
Shed thickness	6
Water layer thickness	1

Table 7 Approximate values of the floating potentials for the insulator with partial wetting

	α_1	α_2
SP floating	80.93	51.71
2D ELFI	81.49	52.74

7 Conclusions

We insistently recommend the formulations which integrate the floating potential directly and the zero flux condition by a constraint. These formulations give better results and are faster than the approximation obtained by a dielectric media with high permittivity because of a smaller number of degrees of freedom and a smaller number of steps of the iterative solver. Thus the additional effort for the implementation of the modified system pays off.

In case of no or small jumps of the permittivity, the indirect approach by the single layer potential and the direct formulation based on the Steklov-Poincaré interface equation give good results. Here the computational times of the single layer approach are smaller.

In case of larger jumps of the permittivity, the direct formulation based on the Steklov-Poincaré interface equation turned out to be superior to the indirect single layer potential ansatz, as the results are of much better quality. In particular, the indirect approach shows unphysical singularities close to edges and corners in the case of large jumps of the permittivity. Comparing the computational times for a desired accuracy and not for a fixed mesh the Steklov-Poincaré formulations turns out to be faster.

Competing interests
The authors declare that they have no competing interests.

Authors' contributions
All authors contributed equally to the writing of this paper. All authors read and approved the final manuscript.

Author details
[1]Institut für Numerische Mathematik, Technische Universität Graz, Steyrergasse 30, Graz, 8010, Austria. [2]Corporate Research, ABB Switzerland Ltd., Baden-Dättwil, 5405, Switzerland.

Acknowledgements
This work was supported by the FP7 Marie Curie IAPP Project CASOPT (Controlled Component and Assembly Level Optimisation of Industrial Devices, www.casopt.com).

Received: 17 April 2014 Accepted: 12 October 2014 Published: 30 Oct 2014

References

1. Roman F, Cooray V, Scuka V: **Comparison of the breakdown of rod-plane gaps with floating electrode**. *IEEE Trans. Dielectr. Electr. Insul.* 1998, **5**(4):622-624.
2. Blaszczyk A, Steinbigler H: **Region-oriented charge simulation**. *IEEE Trans. Magn.* 1994, **30**(5):2924-2927.
3. Singer H, Steinbigler H, Weiss P: **A charge simulation method for the calculation of high voltage fields**. *IEEE Trans. Power Appar. Syst.* 1974, **93**(5):1660-1668.
4. Hsiao GC, Wendland WL: *Boundary Integral Equations*. Berlin: Springer; 2008. [*Applied Mathematical Sciences*, vol. 164.]
5. Sauter SA, Schwab C: *Boundary Element Methods*. Berlin: Springer; 2011. [*Springer Series in Computational Mathematics*, vol. 39.]

6. Steinbach O: *Numerical Approximation Methods for Elliptic Boundary Value Problems. Finite and Boundary Elements*. New York: Springer; 2008.
7. Carstensen C, Kuhn M, Langer U: **Fast parallel solvers for symmetric boundary element domain decomposition equations**. *Numer. Math.* 1998, **79**(3):321-347.
8. Hsiao GC, Steinbach O, Wendland WL: **Domain decomposition methods via boundary integral equations**. *J. Comput. Appl. Math.* 2000, **125**(1-2):521-537.
9. Hsiao GC, Wendland WL: **Domain decomposition in boundary element methods**. In *Fourth International Symposium on Domain Decomposition Methods for Partial Differential Equations, Proc. Symp., Moscow/Russ. 1990*. Philadelphia: SIAM; 1991:41-49.
10. Hsiao GC, Wendland WL: **Domain decomposition via boundary element methods**. In *Numerical Methods in Engineering and Applied Sciences, Part I*. Edited by Alder H, Heinrich JC, Lavanchy S, Onate E, Suarez B. Barcelona: CIMNE; 1992:198-207.
11. Andjelic Z, Of G, Steinbach O, Urthaler P: **Boundary element methods for magnetostatic field problems: a critical view**. *Comput. Vis. Sci.* 2011, **14**:117-130.
12. Andjelic Z, Of G, Steinbach O, Urthaler P: **Fast boundary element methods for industrial applications in magnetostatics**. In *Fast Boundary Element Methods in Engineering and Industrial Applications*. Edited by Langer U, Schanz M, Steinbach O, Wendland WL. Berlin: Springer; 2012:111-143. [*Lecture Notes in Applied and Computational Mechanics*, vol. 63.]
13. Konrad A, Graovac M: **The finite element modeling of conductors and floating potentials**. *IEEE Trans. Magn.* 1996, **32**(5):4329-4331.
14. Pechstein C: *Finite and Boundary Element Tearing and Interconnecting Solvers for Multiscale Problems*. Berlin: Springer; 2013. [*Lecture Notes in Computational Science and Engineering*, vol. 90.]
15. Toselli A, Widlund O: *Domain Decomposition Methods - Algorithms and Theory*. Berlin: Springer; 2005. [*Lecture Notes in Computational Mathematics*, vol. 34.]
16. Andjelić Z, Smajić J, Conry M: **BEM-based simulations in engineering design**. In *Boundary Element Analysis*. Berlin: Springer; 2007:281-352. [*Lect. Notes Appl. Comput. Mech.*, vol. 29.]
17. Of G, Steinbach O, Wendland WL: **The fast multipole method for the symmetric boundary integral formulation**. *IMA J. Numer. Anal.* 2006, **26**(2):272-296.
18. Greengard L, Rokhlin V: **A fast algorithm for particle simulations**. *J. Comput. Phys.* 1987, **73**:325-348.
19. Steinbach O, Wendland WL: **The construction of some efficient preconditioners in the boundary element method**. *Adv. Comput. Math.* 1998, **9**(1-2):191-216.
20. Steinbach O: **Artificial multilevel boundary element preconditioners**. *Proc. Appl. Math. Mech.* 2003, **3**:539-542.
21. Of G: **An efficient algebraic multigrid preconditioner for a fast multipole boundary element method**. *Computing* 2008, **82**(2-3):139-155.
22. Blaszczyk A: **Region-oriented BEM formulation for numerical computation of electric fields**. In *Scientific Computing in Electrical Engineering SCEE2008*. Edited by Roos J, Costa LRJ. Berlin: Springer; 2010:69-76. [*Mathematics in Industry*, vol. 14.]
23. Andjelic Z, Kristajic B, Milojkovic S, Blaszczyk A, Steinbigler H, Wohlmuth M: **Integral methods for the calculation of electric fields, for application in high voltage engineering**. *Technical report* 10, Scientific Series if the International Bureau, Forschungszentrum Jülich; 1992.
24. International Electrotechnical Commission: IEC Technical Standard 60099-4: *Surge Arresters - Part 4: Metal-Oxide Surge Arresters Without Gaps for A.C. Systems*. 2.2 edition; 2009.

10.1186/2190-5983-4-13
Cite this article as: Amann et al.: Simulation of floating potentials in industrial applications by boundary element methods. *Journal of Mathematics in Industry* 2014, 4:13